Measurement system for determining the magnetic polarizability tensor of small metal targets

Measurement System for Determining the Magnetic Polarizability Tensor of Small Metal Targets

Omar A Abdel Rehim*, John L Davidson, Liam A Marsh, Member, IEEE, Michael D O'Toole,
David W Armitage and Anthony J Peyton, Fellow, IEEE
School of Electrical and Electronic Engineering
The University of Manchester
Manchester, M13 9PL, UK
*Email: omar.abdelrehim@manchester.ac.uk

***Abstract*—This paper presents an apparatus to measure the spectroscopic magnetic response of small metallic objects and deduce the magnetic polarizability tensor. The measured trans-impedances of a .222 Remington rifle cartridge and titanium cube are compared to simulated results and are found to match well providing verification of the method. The eigenvalues of the two objects are calculated and discussed highlighting the potential discriminatory aspect. The results support the proposed use of the eigenvalue spectra to provide subsurface classification and discrimination between landmines and clutter.**

Keywords—electromagentic induction; magnetic polarizability tensor; ERW detection

I. INTRODUCTION

Explosive remnants of war (ERW) remain a significant humanitarian and environmental problem worldwide, posing risk of serious injury and contributes to an annual casualty rate in the thousands [1].The main challenge for landmine detectors has shifted over the last decade towards the classification of metallic content as opposed to detection. Increased sensitivity of metal detectors has meant that modern detectors are capable of detecting low-metal anti-personnel mines up to a depth of 15 cm [2]. However, landmine clearance remains a difficult task that is extremely expensive and time consuming since most environments containing unexploded mines are cluttered with innocuous metallic content. A deminer can be faced with as many as 100 to 1000 inert metal objects for every mine [3]. Therefore it is crucial that reliable and accurate techniques are developed to enable rapid discrimination between clutter items and actual targets of interest. In view of this, recent development has seen the introduction of ground penetrating radar (GPR) to complement electromagnetic induction as a means of discriminating between clutter and threat objects [4]. However, recent studies have demonstrated the potential to classify metallic content by identifying the magnetic dyadic polarizability tensor of detected objects [5], [6].

Typical electromagnetic induction (EMI) sensors are composed of an excitation coil which generates a primary magnetic field and a receive coil used to measure the induced fields caused by interactions with surrounding material. Eddy currents generated in the metallic target as a result of the time-varying primary field are dependent on a number of parameters such as size, shape, material and location. This effect is sometimes referred to as *demagnetization effect* or *secondary field*. Consequently, different targets are expected to exhibit different electromagnetic responses. The object specific information is captured in the magnetic polarizability tensor and hence deducing the value from measured data would provide a means of classification.

This paper looks at the development of an instrument that provides a means of measuring the tensor values of low metal anti-personnel mines. We begin by reviewing the basic theory behind the magnetic polarizability tensor. Following this a description of the experimental set-up used to obtain the electromagnetic responses of test objects is given. Simulations of object responses were run in parallel to measurements to verify the measurements and validate the experiment. Thus a description of the simulation approach and results is provided prior to reporting on experimental results. The deduced values of the tensors are then calculated and compared to one another as well as to simulation results. Finally, we report on the relevance of exploiting the described techniques in this paper to provide a library of tensors for anti-personnel mines and items of metallic clutter.

II. BACKGROUND

The magnetic polarizability tensor is referred to in this paper as $\overleftrightarrow{\mathbf{M}}$ and is composed of a 3x3 symmetrical complex matrix that is frequency dependent. It identifies the EMI response based on the induced dipole moment [5]. The double-arrowed accent represents the dyadic nature rather than a matrix or vector quantity [7].

$$\overleftrightarrow{\mathbf{M}}(f)=\begin{bmatrix} M'_{xx}+jM''_{xx} & M'_{xy}+jM''_{xy} & M'_{xz}+jM''_{xz} \\ M'_{yx}+jM''_{yx} & M'_{yy}+jM''_{yy} & M'_{yz}+jM''_{yz} \\ M'_{zx}+jM''_{zx} & M'_{zy}+jM''_{zy} & M'_{zz}+jM''_{zz} \end{bmatrix} \quad (1)$$

The matrix is symmetrical due to electromagnetic reciprocity, meaning that the matrix only contains 6 unique complex numbers [8]. In theory, the tensor can be deduced from as little as 6 incident angles of the primary field. This is provided that the angles are three orthogonal axes and their cross-diagonals to provide a full view of the object, as demonstrated in Fig. 1. However, a larger number of measurement angles are normally performed to provide confidence in the measurements and the deuced tensor.

The authors would like to thank Find A Better Way for their financial support of this research under the SEMIS programme.

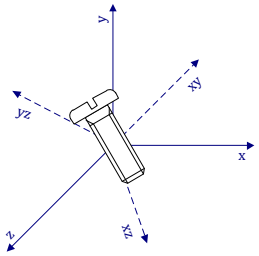

Fig. 1-Example object (screw) and the minimum number of orientations with respect to the primary field required to deduce the tensor.

The tensor $\overleftrightarrow{\mathbf{M}}$ is orientation specific and therefore pre-determined knowledge of the object orientation would be required to perform discrimination. Thus, the Eigenvalue matrix, Λ, is used instead as it provides an orientation-independent means of comparing responses [9]. Λ isolates the three primary orthonormal axis of the object such that an external primary field aligned with one axis would result in a steady state dipole moment parallel to it [10]. It is the spectroscopic information contained in Λ that can be used as a signature to identify and discriminate between mines and clutter. $\overleftrightarrow{\mathbf{M}}$ can be deduced back from Λ to calculate the response in any orientation by applying rotational matrix R, [11], as displayed in (2):

$$\overleftrightarrow{\mathbf{M}} = R \cdot \Lambda \cdot R_T \tag{2}$$

A full derivation of the polarizability tensor theory is provided in [7] and forms the basis of the equation used in this paper. Equation (3) relates $\overleftrightarrow{\mathbf{M}}$ to the measured induced voltage, V_{ind}, in the receive coil of the electromagnetic sensors:

$$V_{ind} = \frac{j\omega\mu_0}{I_R} \vec{\mathbf{H}}_T \cdot \overleftrightarrow{\mathbf{M}} \cdot \vec{\mathbf{H}}_R \tag{3}$$

where $\vec{\mathbf{H}}_T$ and $\vec{\mathbf{H}}_R$ are the fields incident to the object from the transmit and receive coils respectively, μ_0 is the permeability of free space and I_R is the current passing through the receive coil. In practice these equations are used in reverse as the induced voltage is initially measured which provides a means of identifying $\overleftrightarrow{\mathbf{M}}$ which in turn allows the calculation of Λ.

Finally, it is worth noting that in order to approximate the secondary field (the induced voltage) using the field of the magnetic dipole moment, the primary field is assumed to be parallel across the object in question [7]. Additionally, a magnetic dipole approximation may be used to describe a current loop, where the loop dimensions are much smaller than the distance to point of interest [12].

III. Theory

In order to derive $\overleftrightarrow{\mathbf{M}}$ a system needs to be able to provide a parallel primary field at a number of incident angles. Rotating the object within a solenoid coil provides just that. The measurement system makes use of the uniform field within the central region to obtain the measurements required in order to obtain $\overleftrightarrow{\mathbf{M}}$ and ultimately Λ.

Once a set of rotational voltage measurements are obtained, Λ can be obtained by one of two means; *direct calculation* [11] or by *pseudo inversion*. The direct approach can only be applied if the object is highly symmetrical and has a clearly defined primary axes, such as the example screw. The eigenvalue matrix is expected to be composed of a dominant component and two equal smaller values. Hence in theory, only two measurements would be required to obtain the eigenvalues; one with the screw aligned with the field and one with the screw at 90˚. This simplification could go even further to obtain Λ from one measurement if the object responds equally in all directions such as a sphere or cube. Alternatively, for more complex shapes, a full set of rotational measurements needs to be performed and a simple pseudo inversion process can be used to attain the values of $\overleftrightarrow{\mathbf{M}}$. The Jacobian matrix in the inversion is composed of the dot product of values of $\vec{\mathbf{H}}_T$ and $\vec{\mathbf{H}}_R$ for each angle to provide the solution for $\overleftrightarrow{\mathbf{M}}$ as:

$$\overleftrightarrow{\mathbf{M}} = \frac{1}{j\omega\mu_0} J^{-1} \cdot \frac{V_{ind}}{I_T} \tag{4}$$

where J is the Jacobian matrix and I_T is the current through the transmit coil. The induced voltage divided by the transmit coil current is commonly known as the trans-impedance measurement and is the recorded value obtained from the experiment discussed next.

IV. Experimental Setup

A. System Overview

The primary instrument used to perform the measurements is an impedance/gain phase analyser, Solatron SI 1260. The impedance analyser excites the coil with discrete fixed frequencies and captures the trans-impedance values. A bespoke LabVIEW programme controls the measurement process, stepping through the desired frequencies providing the required excitation values and recording the trans-impedance measured by the analyser. This data is then processed using MATLAB to perform the inversion and tensor calculation. Front-end amplification is used to provide a stronger driving current (≈1.2A) and amplify the induced voltage from the receive coil. A system schematic is represented in Fig. 2.

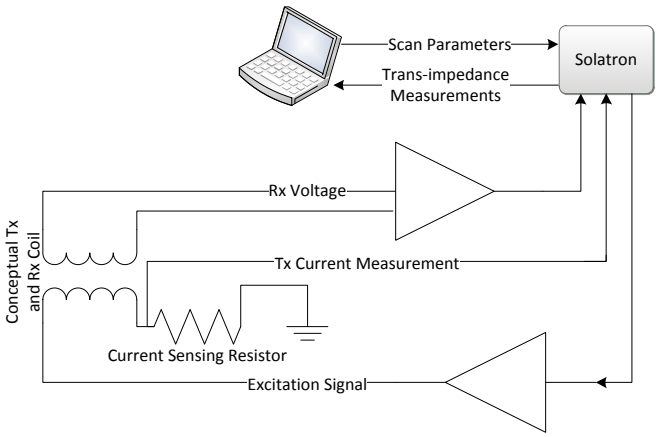

Fig. 2-System schematic highlighting the flow of signals and measurements to and from the Solatron and the workstation.

B. *The coil*

The solenoid coil constructed in order to take the measurements is pictured in, Fig. 3. The coil is composed of an inner 120 turn transmit coil, visualized in red in Fig. 3(a), and two outer 60 turn receive coils wound in a gradiometer arrangement, displayed in green in Fig. 3(a) and red in Fig. 3(b). The coil dimensions are as follows; a=202 mm, b=105 mm, H=220 mm, d=107 mm and D=149 mm, with a wire wall thickness of 1.75 mm for the transmit coil and 1.66mm for the receive. The z-axis is considered to be along the centre of the coil.

The coil was designed to provide maximum sensitivity (larger number of turns) while ensuring the resonance of the coil is well above the region of interest. The frequency range investigated within this paper is 1-100 kHz as this contains the majority of the useful information required for classification.

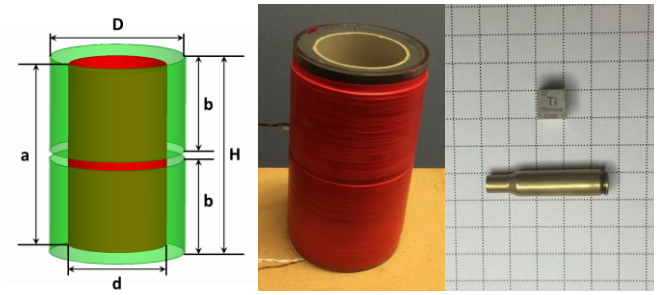

Fig. 3-(a) Coil schematic,(b) constructed coil and (c) test objects used (Titanium cube and .222 Remington shell) on 1 cm grid.

C. *Test Objects*

Fig. 3(c) displays the two test pieces measured within this paper; a .222 Remington rifle cartridge and a titanium cube. The .222 cartridge is made out brass, exact alloy unknown, with a primer assumed to be of the same material (not shown). The cube is made of 10x10x10 mm of pure titanium.

D. *Experimental Procedure*

A mechanical device was used to position the test objects at the most sensitive part of the gradiometer along the z-axis. The device enabled manual rotation for defined angular orientations. In this paper, rotations were performed about the y-axis in 15° steps. Due to the parallel field provided by the solenoid coil, the measurements obtained when rotating about the x-axis would yield identical results. At each angular orientation a full frequency sweep was completed from 1 to 100 kHz and stored. The object was then rotated and the process repeated until a full 360° rotation was performed.

E. *Calibration*

The raw trans-impedance measurements needed to be calibrated against the response of a ferrite object. This was due to the introduction of phase shifts as a result of the front-end amplification as well as an uneven amplification across the frequency range. In order to do so, trans-impedance measurements of a ferrite rod, 6x20 mm, were performed. Ferrite should provide a flat response across the frequency spectrum in terms of magnitude and introduce no phase shift. This information was used to effectively cancel out any errors introduced due to amplification.

F. *Post-Processing and Field Measurement*

A MATLAB programme was used to perform the post processing and calculate the tensor/Eigenvalue matrix. The programme performs the calibration initially to provide a view of the trans-impedance response of the object. As will be seen later this information can be used to deduce information about the object material, size and symmetry. The results are then inverted to deduce the tensor values, and subsequently Λ. As highlighted in section III, this requires knowledge of the field values from of the transmit and receive coils, $\vec{\mathbf{H}}_T$ and $\vec{\mathbf{H}}_R$ respectively. These fields were calculated from flux density measurements using a Hall probe positioned at what would be the metallic object's centre whilst passing a unit current through the transmit and receive coils in turn.

V. Simulation

Simulations were performed using the commercial FEM (Finite Element Method) solver, Ansys Maxwell v16. The simulation geometry comprised of an outer free-space region, the coil arrangement as shown in Fig. 3(a) and the test object positioned nominally at the most sensitive region of the gradiometer. A series of simulations involved geometrical rotations of the test object about its centre in 15˚ increments from 0˚ to 345˚ over the frequency sweep range 1 kHz to 10 kHz in 1 kHz steps and thereafter in 5 kHz steps up to 100 kHz. The geometry of the .222 Remington case was simplified as three stacked geometrical primitives; a long and thin tapered cone, a smaller fatter cone and a simple cylinder representing the outer main body, shoulder and neck respectively of the cartridge. Subtraction of smaller sized primitives enabled the creation of a simplified cartridge shell of 0.5 mm wall thickness. Typical total meshing levels was in the order of 700k tetrahedral elements and solution times for all frequencies and rotations was in the order of 72 hrs running on Intel Xeon ES-2620 (2 GHz) and required approximately 40 GBytes of physical RAM. An example H-field plot of the cartridge shell in the coil arrangement for a simulation of 20 kHz excitation current and angular orientation of 0˚ to the z-axis is shown in Fig. 4.

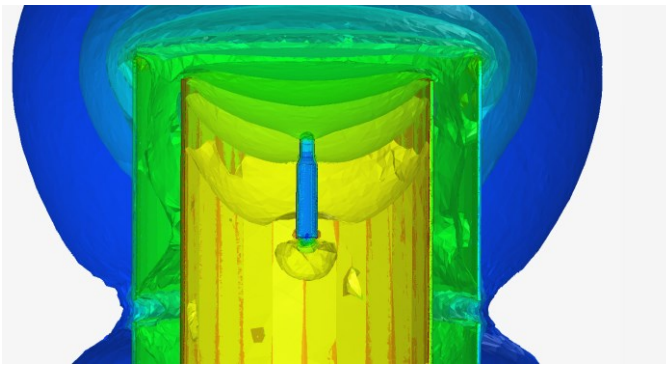

Fig. 4-Cross-sectional upper half of gradiometer showing an example H field perturbation due to the modelled .222 Remington rifle cartridge. Midpoint of the cartridge is at the simulated rotational centre and the most sensitive part of the gradiometer.

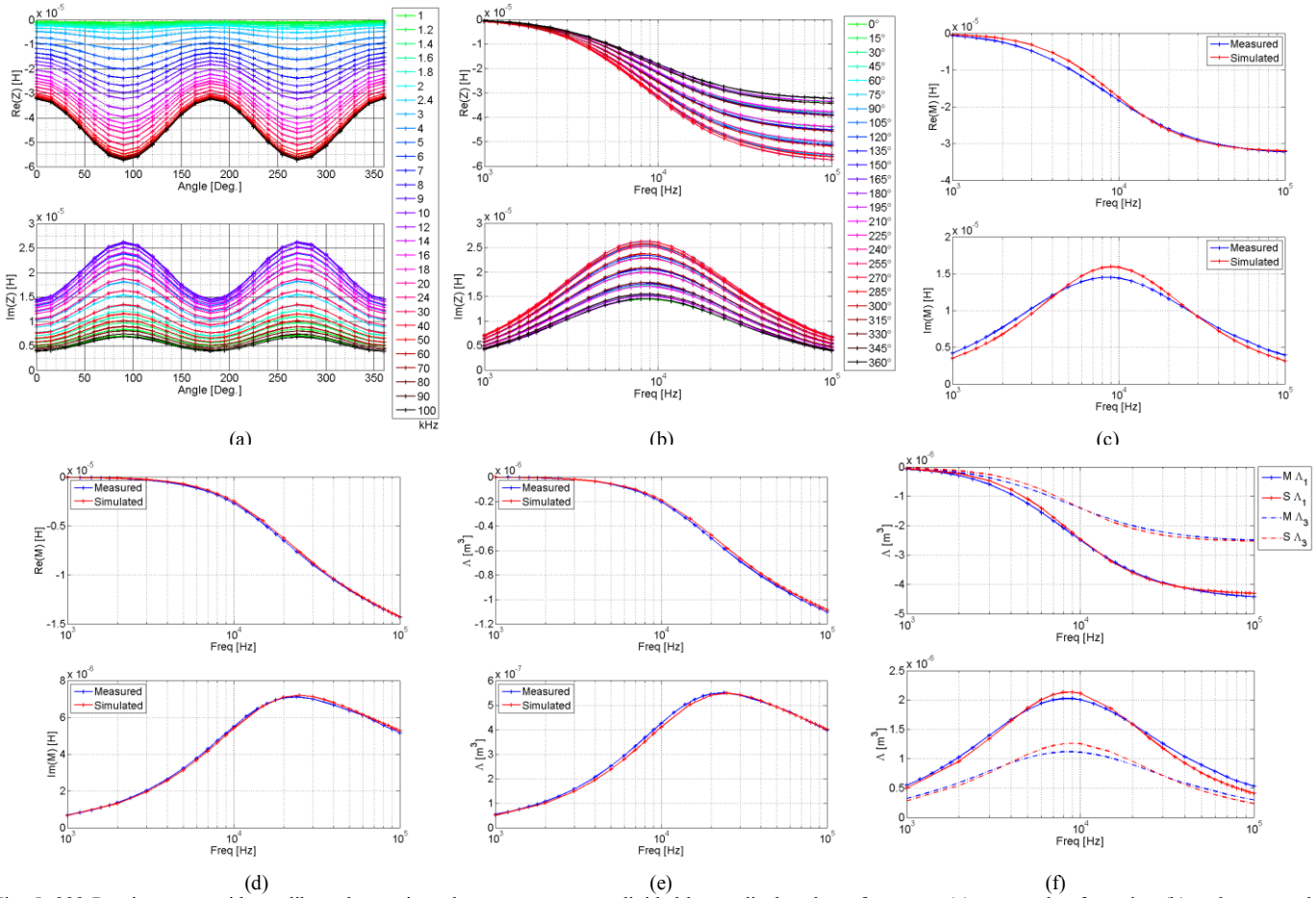

Fig. 5-.222 Remington cartridge calibrated trans-impedance measurement divided by ω, displayed per frequency (a), per angle of rotation (b) and compared to simulated at 0˚ (c). (d) is the comparison between measured and simulated data for the Titanium cube at 0˚. The calculated eigenvalues for the titanium cube (e) and the .222 Remington rifle cartridge (f) for both the measured (blue) and simulated (red) results.

VI. Results and Discussion

A. Trans-Impedance Measurements

The calibrated trans-impedance measurements obtained from the .222 Remington cartridge are presented in Fig. 5. The plots highlight expected results such as the sinusoidal shaped response in (a) which is a result of the geometrical shape of the cartridge. The frequency response displayed in (b) elucidates a number of object specific information such as the material and size. The lack of a positive real response at low frequencies alludes to the lack of ferritic composition in the material. The location of the peak frequency of the imaginary response can be viewed as a function of conductivity. This will be discussed further when comparing the eigenvalues of the cube and cartridge. The smooth measurement transition as the object is rotated can be viewed as a merit to the quality of measurements and they proved to be very reproducible, within 5%.

The measurements were compared with simulated results at 0˚and were found to match very well, Fig. 5(c). However, some slight discrepancies are visible. This is assumed to be down to a number of aspects. Firstly, the simulation lacked the exact material properties of the cartridge; mainly the conductivity of the brass alloy composition was not accurately known. Secondly, there were a number of subtle simplifications to the simulated cartridge such as the absence of the extractor groove and primer. Finally, the cartridge was modelled to have a thicker wall to reduce the number of elements created by the simulation. To confirm these assumptions were the cause of the difference, the titanium cube measurements were compared with simulated data and were found to agree much better as shown in Fig. 5 (d). In this instance, the simulation geometry was modeled far more closely to the physical reality due to the inherently less complex shape of the cube.

B. Eigenvalue matrix

Finally, the Eigenvalue matrix was deduced from the measured and simulated results using the inversion technique described in the section III. The calculated eignevalues from the titanium cube and .222 cartridge for both measured and simulated results are shown in Fig. 5(e) and Fig. 5(f) respectively. Only one eigenvalue is reported for the titanium cube as it responds equally in all directions (the three primary axis) and as result has the same eigenvalue in all three directions. Two eigenvalues are reported for the .222 cartridge; the dominant value (along the length of the cartridge) and a smaller eigenvalue which is identical for the remaining two axes due to its shape. These statements in their own right are discriminatory properties highlighted by the eigenvalue matrix. The identification of the shape of the object alone could potentially provide a means of disregarding clutter.

The peak frequency for the eigenvalue imaginary spectrum provides information about the material properties. The conductivity of the materials is significantly different; brass is typically assumed to have a conductivity of $1.5x10^7$ S/m, while titanium has a considerably lower conductivity of $1.8x10^6$ S/m. This is reflected in the peak position in Fig. 5(e) and Fig. 5(f) where the .222 Remington rifle cartridge displays a peak at around 8 kHz and the titanium cube is around 25 kHz. Finally, the magnitude of the eigenvalue matrix is considerably different highlighting the difference in size. However, the magnitude is a function of the conductivity, permeability and size of the object. Thus it cannot be used as a measure of size, unless prior knowledge of the material is present. Fig. 5(e) and (f) illustrate the potential information that can be deduced about the object. It can be referred to as an object signature and can deliver a discriminating dimension to metal detectors.

VII. Conclusions and Further work

The magnetic dipole polarizability tensor is of great interest in order to identify subsurface targets detected during mine clearance. The instrument described in this paper is capable of performing clean reliable measurements to obtain tensor values of small metal targets. The agreement with simulation results without the need of scaling validates the true tensor values obtained rather than assessing them comparatively. Looking forward the instrument is ready to be used to start measuring the magnetic responses of low-metal metal mines and typical clutter items to provide a library of signatures that can be used by detectors to identify and discriminate. The instrument can also be used to understand the effects of ageing on the response of a mine as well as recognizing the degree to which surrogates reflect the true response of a mine.

Acknowledgment

The authors would like to thank Christos Ktistis and Bachir Dekdouk, formerly of the University of Manchester, for their contribution to this work.

References

[1] "Landmine Monitor 2013," Intl. Camp. to Ban Landmines. Nov. 2013

[2] A. M. Lewis, T. J. Bloodworth, D. M. Guelle, F. R. Littmann, A. Logreco, and M. A. Pike, "Systematic Test & Evaluation of Metal Detectors (STEMD) Interim Report Laboratory Tests Italy," The Inst. for the Protection and Security of the Citizen, Euro. Com. Joint Research Centre, 2006.

[3] MacDonald, J., J. R. Lockwood, J. McFee, T. Altshuler, T. Broach, L. Carin, R. Harmon, C. Rappaport, W. Scott, and R. Weaver , "Alternatives for Landmine Detection", RAND, p. 9, 2003.

[4] K. Koppetsch, J. Glattbach, "Metal Detectors and PPE Catalogue 2007," Geneva Intl. Ctr. for Humanitarian Demining, 2007, p. 4.

[5] Bell, T.H., Barrow, B.J., Miller, J.T. Subsurface Discrimination Using Electromagnetic Induction Sensor. GeoSci. and Rem. Sens. IEEE Trans. vol. 39 No 6, 1286 - 1293 doi: 10.1109/36.927451, 2001.

[6] Makkonen J., Marsh L.A., Vihonen J., Jarvi A., Armitage D.W., Visa A. and Peyton A.J. KNN classification of metallic targets using the magnetic polarizability tensor Meas. Sci. Technol. vol. 25 055105 doi:10.1088/0957-0233/25/5/055105, 2014.

[7] Marsh L.A., Ktistis C., Jarvi A., Armitage D.W. and Peyton A.J. Three-dimensional object location and inversion of the magnetic polarisability tensor at a single frequency using a walk-through metal detector Meas. Sci. Technol. vol. 24 045102 doi:10.1088/0957-0233/24/4/045102, 2013.

[8] Norton S. J., Won I. J. Identification of Buried Unexploded Ordnance From Broadband Electromagnetic Induction Data. GeoSci. and Rem. Sens. IEEE Trans. vol. 39 No 10, 2253 - 2261 doi: 10.1109/36.957288, 2001.

[9] Marsh L.A., Ktistis C., Jarvi A., Armitage D.W. and Peyton A.J. Determination of the magnetic polarizability tensor and three dimensional object location for multiple objects using a walk-through metal detector Meas. Sci. Technol. vol. 24 045102 doi:10.1088/0957-0233/24/4/045102

[10] Fernandez J.P., Barrowes B.E., Grzegorczyk T.M., Lhomme N., O'Neill K., and Shubitidze F. Man-Portable Vector Sensor for Identification of Unexploded Ordnance IEEE Sens. Jr. vol. 11 No. 10, 2542 – 2555 doi: 10.1109/JSEN.2011.2118200

[11] Zhao Y., Yin W., Ktistis C., Butterworth D., and Peyton A.J. On the Low-Frequency Electromagnetic Responses of In-line Metal Detectors To Metal Contaminants Instr. and Meas. IEEE Trans. vol. PP No. 99 doi: 10.1109/TIM.2014.2324791

[12] Ulaby F T, Michielssen E and Umberto R 2010 Fundamentals of Applied Electrodynamics ed A Gilfillan (Englewood Cliffs, NJ: Prentice-Hall) p 261